



New Insights on Betic Cordillera Structure from Gas Geochemistry

C. Lix, P. Zuddas, C. Inguaggiato, X. Guichet, J. Benavente, M. Barbier

► To cite this version:

C. Lix, P. Zuddas, C. Inguaggiato, X. Guichet, J. Benavente, et al.. New Insights on Betic Cordillera Structure from Gas Geochemistry. *Geochemistry, Geophysics, Geosystems*, 2018, 19 (12), pp.4945-4956. <10.1029/2018GC007712>. <hal-01941034>

HAL Id: hal-01941034

<https://hal.science/hal-01941034v1>

Submitted on 30 Nov 2018

HAL is a multi-disciplinary open access archive for the deposit and dissemination of scientific research documents, whether they are published or not. The documents may come from teaching and research institutions in France or abroad, or from public or private research centers.

L'archive ouverte pluridisciplinaire **HAL**, est destinée au dépôt et à la diffusion de documents scientifiques de niveau recherche, publiés ou non, émanant des établissements d'enseignement et de recherche français ou étrangers, des laboratoires publics ou privés.



HAL Authorization

New Insights on Betic Cordillera Structure from Gas Geochemistry

C. Lix^{1,2,3}, P. Zuddas², C. Inguaggiato⁴, X. Guichet¹, J. Benavente³ and M. Barbier¹

¹ IFP Energies Nouvelles, 1 et 4 avenue de Bois-Préau, 92852 Rueil-Malmaison, France.

² Sorbonne Université, CNRS-INSU, Institut des Sciences de la Terre de Paris, ITeP UMR 7193, F-75000 Paris, Campus Pierre et Marie Curie - 4 place Jussieu 75005 Paris, France.

³ Departamento de Geodinámica e Instituto de Investigación del Agua, Universidad de Granada, Granada, Spain.

⁴ Departamento de Geología, Centro de Investigación Científica y de Educación Superior de Ensenada (CICESE), Carretera Ensenada-Tijuana 3918, Ensenada, Baja California, México.

Corresponding author: Claire Lix (claire.lix@sorbonne-universite.fr)

Key Points:

- In central Betic Cordillera, helium isotopic compositions of bubbling and dissolved gases have a dominant radiogenic component.
- Transport mechanisms of fluid within the crust have been evaluated.
- The observed mantle-derived He could result from fossil mantle contribution associated to crustal production from Li-rich rocks.

This article has been accepted for publication and undergone full peer review but has not been through the copyediting, typesetting, pagination and proofreading process which may lead to differences between this version and the Version of Record. Please cite this article as doi: 10.1029/2018GC007712

Abstract

The current lithospheric structure of the Betic Cordillera results from active geodynamic system related to slab retreat slowdown in western Mediterranean. A sharp change in lithospheric thickness has been imaged beneath the Betic Cordillera, potentially resulting from a near-vertical subduction-transform-edge-propagator fault (STEP) towards the surface with possible mantle influx. In this study, we use helium isotopic composition of bubbling and dissolved gases in groundwater samples of the central part of the Betic Cordillera to evaluate the origin of gases and to set constraints on its lithospheric structure. We found that helium isotopic composition have a dominant radiogenic component with a mantle-derived He contribution reaching mainly 1 % for the investigated area. Estimation of He diffusion within the ductile crust indicates that this process is potentially too slow to explain the low mantle-derived He contribution measured at the surface. A new analysis of the available data of the crustal metamorphic complexes allows us to suggest that the crust could be dissociated from the mantle with no evidence of asthenospheric influx. The weak mantle He signature could reflect a mantle material earlier incorporated in the crustal metamorphic complexes of the Betic Cordillera during their exhumation. In light of mass-balance calculations, we propose that the slight ^3He excess observed in the present-day fluids might result from a fossil mantle signature diluted by local radiogenic production over time.

1 Introduction

The Betic Cordillera (Spain) corresponds to the Western European region of the Alpine peri-Mediterranean orogenic belt and forms the Gibraltar arc with the Rif (Morocco) enclosing the Alboran Sea. This region results from the convergence of the Iberian and African plates since the Mesozoic. Several hypotheses have been proposed to explain the geometry and the formation of this tightly arcuate structure including convective removal of thickened continental lithosphere (Platt & Vissers, 1989), delamination of subducted continental lithosphere (Calvert et al., 2000), and slab rollback (Faccenna et al., 2004; and reference therein). Recent tomographic studies supports the theory of slab rollback with (Heit et al., 2017; Mancilla et al., 2015) or without lithospheric delamination (Spakman & Wortel, 2004). The present position of the slab involves a westward slab tearing beneath the Betic Cordillera resulting in large variations of the lithospheric thickness (Mancilla et al., 2015). The Betic Cordillera lithosphere corresponds to a transition zone between the thick Iberian crust and the

thin Alboran crust. Mancilla et al. (2018) have recently suggested that this sharp transition would result from a near-vertical subduction-transform-edge-propagator fault (STEP) spreading towards the surface as a flower-shaped tectonic structure in the crust. In contrast, Rosell et al. (2011) proposed that lithospheric tearing might have resulted in a hot asthenospheric material intrusion displayed by a low-resistivity anomaly beneath the cordillera at shallow depth (< 50 km). Both the anomaly and the transition between thick and thin lithospheres are located beneath the Granada Basin and the Sierra Nevada. This area is also characterized by recent active tectonic movements and low to medium enthalpy geothermal springs historically used as thermal baths (*baños*) (Bufo et al., 2004; López-Chicano et al., 2001).

In this work, we investigate the noble gas isotopic composition of fluids of the Betic Cordillera to refine our understanding on the structural relationship between mantle, ductile lower crust, and fragile upper crust. Noble gases are inert elements and thus their isotopic composition reflect that of the fluid sources making them excellent tracers of fluids origin (Ballentine et al., 2002). Terrestrial atmosphere, mantle, and crust have distinct helium isotopic ratios. ^3He is a primordial isotope acquired during the Earth accretion and enriched in the mantle over ^4He . This latter is continuously produced by radiogenic decay of U, Th in the crust (Ballentine & Burnard, 2002). Here, we present a study of the chemical composition and helium isotopes of bubbling and dissolved gases in groundwater in the central Betic Cordillera and analyze possible origin of fluid composition in this complex tectonic region.

2 Geological settings and tectonic framework of the Betic Cordillera

Our sampling area is located in the tectonically active central region of the Betic Cordillera, with a concentration of sampling points in the Granada Basin to the west of the Sierra Nevada massif. Presently, westward tectonic movement actively deforms the Sierra Nevada with higher displacement in the western part (Galindo-Zaldívar et al., 2015). The Granada Basin is an active Neogene intramountainous basin in the Betic Cordillera with NW–SE to NNW–SSE normal faults dipping westwards.

Two main parts may be distinguished into the complex structure of the Betic Cordillera: (1) the Iberian Domain including the non-metamorphic External Zone and (2) the Alboran Domain corresponding to the metamorphic Internal Zones (Figure 1a). The External Zone is separated from the Internal Zone by a major shear zone called the Internal External Boundary Zone (IEBZ, Figure 1) (Sanz de Galdeano, 1990). In the NE part of the Granada Basin, this

tectonic accident becomes nearly coincident with the so-called Cadix-Alicante faults system (CAFS, Figure 1a and 1b) extending from 550 km across the Betic Cordillera. This fault system represents one of the major tectonic accidents in the region with crustal discontinuity exceeding 7 km depth (Sanz de Galdeano, 2008 and references therein). Another significant tectonic accident of concern in this study is the so-called Alpujarras fault corridor (AFC, Figure 1a and 1b), which has a general E-W dextral strike-slip component and limits the Sierra Nevada massif to the south. The cross-sections I-I' and II-II' (Figure 2a and 2b) illustrates the westward termination of the Sierra Nevada massif at lithospheric scale. The cross-section I-I' (Figure 2a) has been drawn by compiling current interpretations of previous geophysical investigations (Mancilla et al., 2015, 2018, Palomeras et al., 2017; Thurner et al., 2014) and Moho depths determined by Diaz et al. (2016). The cross-section II-II' (Figure 2b) has been modified from Crespo-Blanc and Frizon de Lamotte (2006).

2.1 Iberian Domain

The Iberian Domain is composed of a hercynian basement (Iberian Meseta) and the External Zone, which corresponds to the Iberian paleo-margin cover and is made up of sedimentary rocks deformed into fold-and-thrust belt during the early Miocene (Crespo-Blanc & Frizon de Lamotte, 2006). The Iberian Domain is characterized by a variable crustal thickness increasing from 35 to 40 km from west to east respectively (Diaz et al., 2016; Mancilla et al., 2015). The transition between the fragile upper crust and the ductile lower crust occurs at around 20 km (Fernández-Ibáñez et al., 2005).

2.2 Alboran Domain

The Alboran Domain or Internal Zone consists of three stacked metamorphic complexes distinguished from top to bottom by variable metamorphic degree: (1) the Maláguide with low grade metamorphism of greenschist facies (García-Tortosa et al., 2000); (2) the Alpujárride with HP/LT metamorphism of blueschist facies (Azañón & Crespo-Blanc, 2000); and (3) the Nevado-Filábride with HP/LT metamorphism of eclogitic and blueschist facies (Gómez-Pugnaire & Fernández-Soler, 1987). The accretion and the exhumation of the Alboran Domain occurred during the pre-Miocene intracontinental collision and the early Miocene extensional phase, respectively (Azañón & Crespo-Blanc, 2000; Martínez-Martínez & Azañón, 1997). This accretion event was coeval with thin-skinned thrusting of the External

Zone. During the Miocene exhumation, the metamorphic complexes were re-organized by low-angle normal faults shaping the present-day upper crust (Booth-Rea et al., 2004). The base of the Alpujárride Complex in the western part of the Betic Cordillera is characterized by the presence of structurally intercalated bodies of peridotite (Tubía et al., 1992) (Figure 1a). Today, the depth of Alboran Domain Moho is estimated to be at ~ 20-25 km depth (Díaz et al., 2016; Mancilla et al., 2015).

2.3 Neogene Basins

The Iberian and Alboran domains are the basement of several intramountainous basins (e.g. Tabernas, Sorbas, Guadix-Baza, Granada), which were formed during the last ~13 Myr (Braga et al., 2003). The infilling of these basin includes a variety of rocks, mainly clayey conglomerates, calcareous sandstones, marls and silts, gypsum/anhydrite (and locally halite), lacustrine limestones, cemented breccias and alluviums from bottom to top. Significant southwestward displacement is currently observed in the Granada Basin due to extensional deformation, whereas the eastern basins display low movements (Galindo-Zaldívar et al., 2015).

3 Materials and Methods

3.1 Sample location

We sampled bubbling and dissolved gases in twelve locations of the central Betic Cordillera. Nine springs and three wells were selected over ~ 200 km along the main tectonic boundaries (Figure 1b). Baño Salado de Lanjaron and Capuchina de Lanjaron springs (points 1 and 2) are located in the Sierra Nevada along the detachment between Nevado-Filábride and Alpujárride complexes. Baños Alhamilla spring (point 3) is situated further to the east in the Sierra Alhamilla along the same tectonic contact, where it intersects the trace of an important strike-slip fault of near N30E direction. Baños de Zujar, Baños de Alicun de las Torres, Frontil, Sierra Elvira, and Vivero Arco (points 4 to 8) are close to the above mentioned CAFS. The two last points of this group (7 and 8) are also located on the trace of an active fault, belonging to the NW to NNW directed fault system that continues toward the city of Granada. Baños Santa Fe, Salinas la Malaha, Baños Urquizar Grande (points 9 to 11) are also aligned along a fault striking N30E. Finally, Baños Alhama de Granada (point 12), Baños Santa Fe (point 9) are presumably close to the IEBZ.

3.2 Sampling

At every sampling point, physico-chemical parameters of the waters, including temperature, pH, alkalinity and electrical conductivity (EC) were measured. The collected samples correspond to eleven waters and four bubbling springs.

Waters were collected by filling 142 mL and 242 mL Pyrex glass bottles to analyze chemical composition and helium isotope composition, respectively, of dissolved gases (Capasso & Inguaggiato, 1998; Inguaggiato & Rizzo, 2004). The glass bottles were sealed under water with silicon/rubber septa to minimize the atmospheric contamination (Capasso & Inguaggiato, 1998).

The bubbling gas samples were collected using an upside-down funnel submerged in the water and connected to a three-way valve. The gas accumulated in the funnel was sucked and pushed in the glass flasks (equipped with two vacuum stopcocks) through a syringe connected to the three way valve (Inguaggiato et al., 2016, and references therein).

3.3 Laboratory gas analyses

Laboratory gas analyses were carried out at the *Istituto Nazionale di Geofisica e Vulcanologia* - Palermo (Italy). Dissolved gases were extracted following the method described by Capasso and Inguaggiato (1998) and Inguaggiato and Rizzo (2004). A known volume of host gas was injected into the upside-down glass bottles while drawing out the equivalent water volume through needles. After equilibration for 24 hours allowing the equilibrium partition of gas species between the liquid phase and the host gas phase, a variable gas volume was extracted for analyses by injecting water into the glass bottles. Elemental and isotopic gas analyses were performed in 15 days from the date of sampling. Gas species (O_2 , N_2 , CH_4 , CO_2 and He) were analyzed by gas chromatography (Clarus 500, Perkin Elmer instrument with Carboxen 1000 columns with a hot wire detector and a flame ionization detector) using Ar carrier gas. The composition of dissolved gases, expressed in cm^3 (STP)/ L_{water} , was calculated taking into account the volume of gas extracted, the volume of water sample, and the solubility of each gas species (Bunsen coefficient in cm^3_{gas} (STP)/ L_{water}). The composition of bubbling gases was expressed in either % vol or ppmv. The uncertainty (1σ) for elemental gases determination is within 5 %.

The gas mixture was purified in a stainless steel preparation line in order to remove all the species except noble gases. He and Ne were then separated from each other by a cryogenic trap first cooled down to $-263.15^\circ C$ to adsorb both species, second rising the temperature at -

233.15°C to release helium and to -193.15°C to release neon, and finally separately admitted into the appropriate mass spectrometers. Helium isotope composition and ^{20}Ne concentration were determined by a GVI-Helix SFT mass spectrometer and a ThermoFisher-Helix MC plus multi-collector mass spectrometer respectively (Rizzo et al., 2016, and references therein).

For each analytical session, we analyzed at least one standard of He and Ne that had previously been purified from air following the above procedure of separation by cryogenic trap. The uncertainty (1σ) of the $^3\text{He}/^4\text{He}$ ratio is 3 %, while for ^4He and ^{20}Ne is 5 % for both free or dissolved gases. The $^3\text{He}/^4\text{He}$ isotopic ratio, R , was normalized to atmospheric composition ($R_A = 1.384 \times 10^{-6}$; Clarke et al., 1976) and then corrected for the atmospheric contamination using the following equation:

$$(R/R_A)_c = [(R/R_A)_s * X - 1]/(X - 1) \quad (1)$$

where R is the measured ($^3\text{He}/^4\text{He}$) isotopic ratio, R_A is the air ($^3\text{He}/^4\text{He}$) isotopic ratio, the subscripts s and c refer to measured and corrected ratios respectively, and X , corresponding to a proportionality factor between the sample and the air isotopic contribution, is estimated by:

$$X = \left(\frac{^4\text{He}}{^{20}\text{Ne}}\right)_s / \left(\frac{^4\text{He}}{^{20}\text{Ne}}\right)_{\text{air}} \times \beta_{\text{Ne}}/\beta_{\text{He}} \quad (1a)$$

where β are the Ne and He Bunsen coefficients (Weiss, 1971).

4 Results

4.1 Fluid composition

Temperatures of the sampled fluids were between 17°C and 51°C with the lowest values observed in the central part of the Granada Basin (Salinas la Malaha and Vivero Arco, 17°C and 20°C respectively). All water samples have EC, pH and alkalinity values ranging from 1.5 to 187.1 mS/cm, 5.8 to 7.4 and 2.53×10^{-3} to 1.29×10^{-2} mol/L respectively. High EC were observed in water samples located near the evaporitic rocks of the Granada Basin. Capuchina de Lanjaron differs from the others sampling points because of higher alkalinity (1.29×10^{-2} mol/L) and lower pH (6.1).

The chemical composition of dissolved and bubbling gases is displayed in Figure 3. We found that the proportion of CO_2 is close to 15 % in the sedimentary Granada Basin and reaches 50 % along the Cadix-Alicante fault system. Baños Salado and Capuchina de

Lanjaron springs, located near the detachment between the Nevado-Filábride and the Alpujarride complexes, have more than 95 % of CO₂.

4.2 Noble gases

The concentration and isotopic composition of He are reported in Table 1. In both dissolved and bubbling gases, we found that He concentration ranges by two orders of magnitude reaching values up to $5.34 \times 10^{-3} \text{ cm}^3 \text{ (STP)/L}_{\text{water}}$ and 120.76 ppmv respectively and are significantly higher compared to both air-saturated water (ASW) and air. We found that He concentration exceeds $1.46 \times 10^{-3} \text{ cm}^3 \text{ (STP)/L}_{\text{water}}$ when the water temperature is above 30°C, whereas it is lower than $6.21 \times 10^{-4} \text{ cm}^3 \text{ (STP)/L}_{\text{water}}$ when water temperature is under 25°C. The helium isotopic composition of the dissolved gases ranges from 0.06 to 0.44 R_A, while ³He/⁴He in bubbling gases spans from 0.11 to 1.03 R_A. The ⁴He/²⁰Ne ratio ranges from 0.40 to 32.87 and 0.46 to 10.46 for dissolved and bubbling gases, respectively. Four samples have a ⁴He/²⁰Ne ratio lower than 1, reflecting a He atmospheric contribution of more than 20 %. The air-corrected helium isotopic compositions (³He/⁴He)_c of both dissolved and bubbling gases display much lower values, ranging from 0.017 ± 0.007 to 0.106 ± 0.004 R_A.

Plotting the measured ³He/⁴He ratio versus the ⁴He/²⁰Ne ratio for both dissolved and bubbling gas samples (Figure 4), we found that our samples can be described by a mixing proportion between three end-members: air or ASW, crust, and mantle. We assume that the crust end-member has a ³He/⁴He ratio value of 0.02 ± 0.01 R_A (Sano & Marty, 1995) and a ⁴He/²⁰Ne ratio ranging from 900 to 10,000 (Sano & Wakita, 1985). The mantle ³He/⁴He ratio is here assumed to be equivalent to that of the sub-continental lithospheric mantle (SCLM) of 6 ± 0.9 R_A (Gautheron & Moreira, 2002). The atmosphere-derived ratios are well constrained (³He/⁴He = 1 ± 0.0009 R_A and ⁴He/²⁰Ne = 0.318 for air; ³He/⁴He = 0.983 R_A and ⁴He/²⁰Ne = 0.285 for ASW; Benson & Krause, 1980 and Ozima & Podosek, 2002). However, excess of air might be present in water due to bubbling effect with consequent lowering of the ⁴He/²⁰Ne ratio down to 0.19 (Gilfillan et al., 2011; Kipfer et al., 2002).

Plotting our data on mixing lines between air-crust-SCLM end-members, we found that the majority of He in our fluids results from a mixing of atmosphere-derived and 1 % mantle – 99 % crust end-members with an atmospheric contribution mainly spanning between 1 and 10 % (Figure 4). The uncertainty in the mixing proportion is represented in Figure 4 by the surface area around the hyperbolas.

We estimated more precisely the mantle contribution in the binary mantle/crust system using the constrained mantle and crustal $^3\text{He}/^4\text{He}$ end-members and the air-corrected $^3\text{He}/^4\text{He}$ ratio. The mantle contribution of He in samples AT, SE, BAG, BAA, and BZ varies between 0.5 ± 0.2 and 1.4 ± 0.3 %. The samples VA, FR, BSL, BUG, and SF have a mantle contribution lower than 0.3 ± 0.2 %, fitting on the mixing line between air/ASW and crust end-members (Figure 4). However, we found that Capuchina de Lanjaron, situated on the important regional contact between Alpujarride and Nevado-Filábride complexes has a He mantle contribution of 18 ± 13 % and more than 95 % of CO_2 . The He isotopic ratio could indicate a potential mantle contribution despite the high air proportion.

Estimations of 0.5 to 1.4 % magmatic fluids in 5 samples within the 1σ uncertainty can be considered as a minimum given the possible excess air in water samples and the potential presence of crustal ^{20}Ne . Both assumptions would decrease the air correction and increase the mantle contribution (0.1 % rise assuming the $^4\text{He}/^{20}\text{Ne}$ ratio of our samples to be 30 % higher).

5 Discussion

Helium in surface manifestations along the Betic Cordillera has only 1.4 % maximum mantle contribution. This calls in question which transport mechanism can cause this anomaly. We initially test a simple diffusion mechanism and thus He transport processes that were constrained by tentative mass-balance calculation.

5.1 A possible He diffusion mechanism

We initially test whether diffusion in the ductile lower crust could be a viable transport mechanism for mantle-derived helium. We assume that ^3He diffuses from the mantle into the ductile lower crust before being advected in the upper crust through the major faults. Based on our cross-sections (Figure 2), we estimate the minimum distance (d) for mantle-derived helium to cross the lower crust at 25 ± 10 km. The characteristic time of He degassing can be evaluated considering the thermal event dated at 20 Ma in the Alboran Domain related to the beginning of both extensional phase and metamorphic exhumation (Vergés & Fernández, 2012). Considering a 1D diffusion model, the ^3He concentration within the ductile lower crust has been evaluated by an analytical solution of the diffusion equation expressed by Equation 3:

$$C(z, t) = C_m + (C_s - C_m) \times \text{erf}\left(\frac{z}{2\sqrt{Dt}}\right) \quad (2)$$

where $C(z, t)$ is the ^3He concentration within the ductile lower crust at time (t) and distance from the Moho (z); $C_s = C(d, 0) = 0$ is the initial ^3He concentration at the lower-upper crust limit; $C_m = C(0, t)$ is the mantle-derived ^3He concentration constant, and D is the apparent He diffusion coefficient.

Equation 3 yields an apparent He diffusion coefficient D ranging from 2.7×10^{-8} to $1.5 \times 10^{-7} \text{ m}^2.\text{s}^{-1}$ when considering: the minimum 1 % mantle-derived helium measured at the surface and a time range of 20 Myr (e.g., $C(d, 20 \text{ Myr}) = 1 \% C_m$). To apprehend the validity of this calculation, we compare our estimated apparent He diffusion coefficient to that in minerals and pore waters potentially present in the lower crust. Crystal lattice diffusion is an extremely slow process in minerals like muscovite and hornblende, which could be representative of the lower crust, with helium diffusion coefficient close to $10^{-12} \text{ m}^2.\text{s}^{-1}$ at 500°C (Lippolt & Weigel, 1988). Helium diffusion coefficient in He-rich minerals (eg, apatite, zircon) ranges between 10^{-15} to $10^{-14} \text{ m}^2.\text{s}^{-1}$ at 500°C (Cherniak et al., 2009). These values are more than 5 orders of magnitude lower than our estimated He apparent diffusion coefficient. For pure water, there is no data of He diffusion coefficient at 500°C . However, the diffusion coefficient of ions having a similar radii-sized (i.e., H^+ and Li^+) in water up to 500°C does not exceed $10^{-8} \text{ m}^2.\text{s}^{-1}$ (Oelkers and Helgeson, 1988). The amount of “free water” in the ductile lower crust generally estimated to be less than 1 % (Hyndman & Shearer, 1989) implying that the He diffusion coefficient should be reduced by several orders of magnitude.

The result of this calculation supports the hypothesis that diffusion alone is not efficient enough to transport ^3He from mantle to fragile upper crust in the Betic Cordillera indicating that other mechanisms such as advection and/or convection could control the eventual mantle-derived He transport in this complex geological region.

5.2 Overall He transport and structural evolution of the Betic Cordillera

In order to constrain He transport mechanisms in the area, we scale the previously estimated apparent He transport coefficient to an “advective” velocities (v) using the following Equation 4 (Jähne et al., 1987):

$$v = D/(d\phi) \quad (4)$$

where d is the distance that ^3He would have to cross to reach the surface, ranging from 15 to 35 km, and φ is the porosity assumed to be 1 % (Hyndman & Klemperer, 1989).

According to Equation 4, we found an “advective” velocity, representing the average rate at which ^3He should have crossed the complex crustal structure to reach the surface during the last 20 Myr, ranges from 2.4 to 13.2 mm/yr. The velocity estimated here is on the same order of magnitude of the Nevado-Filábride Complex exhumation rates estimated to be of 0.5 and 2.8 mm/yr (Vergés and Fernández 2012). The complex tectonic and geologic history of the Betic Cordillera is in fact characterized by important vertical displacements of rocks, including burial and exhumation of the metamorphic complexes, since the early Miocene.

Reanalyzing the pressure-temperature exhumation paths of the Alpujárride and Nevado-Filábride complexes from thermo-barometric data of Augier et al. (2005), Azañón and Crespo-Blanc (2000), and Gómez-Pugnaire and Fernández-Soler (1987) we found that: At ~ 20 Ma, the Alpujárride and Nevado-Filábride complexes, previously dragged into the subduction channel, might be located down to 30 and 40 km depth respectively according to thermochronology data (Augier et al., 2005; Janowski et al., 2016, and references therein). Since the Nevado-Filábride Complex was close to the Alboran asthenospheric mantle and heated subducted material allows movement of low viscosity rocks inside the accretionary complex (Jolivet et al., 2003), asthenospheric materials could be easily incorporated. This process is in agreement with the presence of serpentinite layers found in the Nevado-Filábride Complex (Dyja-Person et al., 2018) and is also consistent with the known peridotite massifs and xenoliths, with low $^3\text{He}/^4\text{He}$ values ranging from 1.4 to 5.7 R/R_A , intercalated into the Alpujárride Complex (Martelli et al., 2011; Tubía et al., 1992).

At ~ 15 Ma, the metamorphic complexes were exhumed initially through a ductile shear zone in the lower crust and then through low-angle detachment faults in the fragile upper crust. This two-stage exhumation model proposed here is in agreement with the results of the thermo-mechanical numerical modelling of Burov et al. (2001) and Jolivet et al. (2003). Since the Betic Cordillera crust contain mantle-derived material incorporated during its burial and exhumation history, we propose that the 1 % mantle-derived helium found in the present-day fluids results from a progressive degassing of the paleo-asthenospheric material incorporated in the crust. Our study indicates that convective movements associated with the metamorphic complex exhumation appear to be faster than He diffusion through the lower crust. Nevertheless, the different geodynamic models (slab rollback, delamination of the

lithosphere, and convective removal of thickened continental lithosphere) responsible for the exhumation cannot be still discriminated.

5.3 Constraining ^3He origin by mass balance calculations

Although we cannot exclude a low $^3\text{He}/^4\text{He}$ fractionation during release from minerals (Tolstikhin et al., 1999) to explain the measured He isotopic ratio in the Betic Cordillera, the possible source ^3He could result from both mantle material and crustal production of Li-rich rocks.

To assess the volume of mantle-derived material incorporated into the crust, we ideally use a mass balance approach using ^4He crustal production and the ^3He abundance in xenoliths. To assess the ^4He crustal production, we consider an average upper crust composition ($[\text{U}] = 2.8 \pm 1.3$ ppm and $[\text{Th}] = 9 \pm 3$ ppm) (Rudnick & Fountain, 1995) and a crust density of $2.7 \pm 0.1 \text{ g/cm}^3$. Using Steiger & Jäger (1977)'s decay constants, we find that ^4He crustal production rate is $7.1 \pm 2.9 \times 10^{-11} \text{ mol/m}^3/\text{yr}$. The $[\text{He}]$ in the crust was estimated assuming that the sampled fluids are in closed system conditions with a residence time between 10^3 and 10^5 years. We found that the overall production of ^4He in the crust ranges from 7×10^{-8} to $7 \times 10^{-6} \text{ mol/m}^3$. Since ^3He abundance in mantle-derived materials (MORB and xenoliths) varies between 10^{-14} and $10^{-10} \text{ cm}^3 \text{ (STP)/g}$ (Martelli et al., 2011; Ozima & Podosek, 2002) and assuming a rock density of $3 \pm 0.1 \text{ g/cm}^3$, the $[\text{He}]$ spans between 10^{-12} and 10^{-8} mol/m^3 .

Thus, the average volume of mantle-derived material that would be incorporated into 1 m^3 of current crustal material should be determined by the proportion between the ^3He abundances and 1 % of the estimated ^4He crustal production. Our estimation gives an average volume of mantle-derived material between $3 \cdot 10^{-2}$ and 10^5 m^3 . The result of this calculation gives partially non-realistic values ($\text{volume}_{\text{mantle material}} > \text{volume}_{\text{crustal material}}$). However, the possible minimum value obtained in this estimation may correspond to an eventual MORB signature. This calculation indicates that the He mass-balance modelling cannot be simply constrained by the mantle He hypothesis alone and that Li-rich rocks potentially present in the crust should be invoked as source of ^3He excess.

In rocks like granite, shale, sandstone, and evaporites, the crustal ^3He production, derived from ^6Li concentration, ranges from at least 1.0×10^{-19} to $1.3 \times 10^{-17} \text{ mol/m}^3/\text{yr}$ (Lehmann et al., 2003; Tolstikhin et al., 2011; Tolstikhin et al., 1996). We estimate the complete He

transfer from rock to water under the closed-system assumption, using the following (Tolstikhin et al., 1996) equation:

$${}^4\text{He}_{\text{water}} = {}^4\text{He}_{\text{rock}} \times \left(\frac{1 - \varphi}{\varphi} \right) \times \left(\frac{\rho_r}{\rho_w} \right) \quad (3)$$

where φ is the average porosity assumed to be 3 % for the whole crust, ρ_r is the average rock density assumed to be 2.7 g/cm³ and ρ_w is the average water density assumed to be 1 g/cm³.

We found that the crustal ³He concentration in water would range from 3 x 10⁻¹⁵ to 4 x 10⁻¹¹ mol/m³, whereas the crustal ⁴He concentration in water would be between 1 x 10⁻⁶ and 3 x 10⁻⁴ mol/m³. In Figure 5, we report ³He and ⁴He concentrations in water calculated from crustal production and measured in our samples (4.1 x 10⁻⁶ < ⁴He < 2.4 x 10⁻⁴ mol/m³ and 1.6 x 10⁻¹² < ³He < 2.4 x 10⁻¹¹ mol/m³).

We found that, considering groundwater residence time of 10⁵ yr, the ³He crustal production is in agreement with the measured values while ⁴He crustal production corresponds to the limit of the ⁴He measured values. On the other hand, considering a groundwater residence time of 10⁴ yr, ⁴He crustal production matches the average measured concentrations while ³He crustal production corresponds to the lower boundary of measured values. This suggests that Li-enriched rocks alone cannot constrain the origin of ³He excess.

We finally propose that the ³He signature observed in our samples might result from both crustal production (related to enriched Li content) and incorporation of mantle material during the exhumation of the metamorphic complexes but the proportion of the two potential sources still remains not evaluated.

6 Conclusions

Gas geochemistry from groundwater samples have been investigated for the first time in the central Betic Cordillera. Helium isotopic compositions of bubbling and dissolved gases show that the crustal radiogenic He signal is predominant whereas the mantle-derived He contribution reaches mainly 1 %. The helium isotopic signature is relatively homogeneous at the scale of the metamorphic complexes of the Betic Cordillera, although at Capuchina de Lanjaron where a higher He mantle contribution has been detected. Transport of mantle-derived He by diffusion within the ductile lower crust cannot provide a suitable explanation for the observed 1 % mantle-derived contribution measured at the surface, diffusion being a slow process at geological timescale. Therefore, our results show that the crustal system of

the Betic Cordillera, is currently dissociated from the mantle system. We propose that, during the exhumation of the metamorphic complexes of the Betic Cordillera, incorporation of asthenospheric material might have led to a relative enrichment in ^3He . The presence of xenoliths in the Betic Cordillera support this hypothesis, however He mass balance calculations do not allow excluding ^3He production from crustal Li-rich rocks associated to the fossil mantle signature.

Acknowledgments

The Authors wish to thank L. Jolivet, D. Do Couto, A. Battani, V. Rouchon for helpful discussions during various stages of this study and Juan Antonio Luque for helping during the sampling survey. The Authors are grateful to the Reviewers, Dr. Pinti and Dr. Györe, for their fruitful comments that helped to improve the quality and the clarity of the manuscript. We also appreciate the specific and editorial comments of the Editor, Dr. Faccenna that helped to restructure the discussion of the manuscript. This work was supported by IFPEN and Sorbonne Université. We also thank the Istituto Nazionale di Geofisica e Vulcanologia – Palermo (INGV), especially Andrea Rizzo and Mariano Tantillo for noble gas analyses. The data used in this paper are listed in the main text, tables, and figures.

References

- Augier, R. (2004). *Evolution tardi-orogénique des Cordillères Bétiques (Espagne): Apports d'une étude intégrée*. Université de Pierre et Marie Curie - Paris VI.
- Augier, R., Agard, P., Monié, P., Jolivet, L., Robin, C., & Booth-Rea, G. (2005). Exhumation, doming and slab retreat in the Betic Cordillera (SE Spain): In situ $^{40}\text{Ar}/^{39}\text{Ar}$ ages and P-T-d-t paths for the Nevado-Filabride complex. *Journal of Metamorphic Geology*.
<https://doi.org/10.1111/j.1525-1314.2005.00581.x>
- Azañón, J. M., & Crespo-Blanc, A. (2000). Exhumation during a continental collision inferred from the tectonometamorphic evolution of the Alpujarride Complex in the central Betics (Alboran Domain, SE Spain). *Tectonics*, 19(3), 549–565. <https://doi.org/10.1029/2000TC900005>
- Ballentine, C. J., Burgess, R., & Marty, B. (2002). *Tracing fluid origin, transport and interaction in the crust. Reviews in mineralogy and geochemistry* (Vol. 47). Mineral Soc America.
<https://doi.org/10.2138/rmg.2002.47.13>
- Ballentine, C. J., & Burnard, P. G. (2002). *Production, release and transport of noble gases in the*

- continental crust. Reviews in mineralogy and geochemistry* (Vol. 47). Mineralogical Society of America. <https://doi.org/10.2138/rmg.2002.47.12>
- Benson, B. B., & Krause, D. (1980). Isotopic fractionation of helium during solution: A probe for the liquid state. *Journal of Solution Chemistry*, 9(12), 895–909.
- Booth-Rea, G., Azañón, J. M., & García-Dueñas, V. (2004). Extensional tectonics in the northeastern Betic (SE Spain): Case study of extension in a multilayered upper crust with contrasting rheologies. *Journal of Structural Geology*, 26(11), 2039–2058.
<https://doi.org/10.1016/j.jsg.2004.04.005>
- Braga, J. C., Martín, J. M., & Quesada, C. (2003). Patterns and average rates of late Neogene--Recent uplift of the Betic Cordillera, SE Spain. *Geomorphology*, 50(1–3), 3–26.
[https://doi.org/10.1016/S0169-555X\(02\)00205-2](https://doi.org/10.1016/S0169-555X(02)00205-2)
- Bufo, E., Bezzeghoud, M., Udías, A., & Pro, C. (2004). Seismic Sources on the Iberia-African Plate Boundary and their Tectonic Implications. *Pure and Applied Geophysics*, 161, 623–646.
<https://doi.org/10.1007/s00024-003-2466-1>
- Burov, E., Jolivet, L., Le Pourhiet, L., & Poliakov, A. (2001). A thermomechanical model of exhumation of high pressure (HP) and ultra-high pressure (UHP) metamorphic rocks in Alpine-type collision belts. *Tectonophysics*, 342(1–2), 113–136. [https://doi.org/10.1016/S0040-1951\(01\)00158-5](https://doi.org/10.1016/S0040-1951(01)00158-5)
- Calvert, A., Sandvol, E., Seber, D., Barazangi, M., Roecker, S., Mourabit, T., et al. (2000). Geodynamic evolution of the lithosphere and upper mantle beneath the Alboran region of the western Mediterranean: Constraints from travel time tomography. *Journal of Geophysical Research: Solid Earth*, 105(B5), 10871–10898. <https://doi.org/10.1029/2000JB900024>
- Capasso, G., & Inguaggiato, S. (1998). A simple method for the determination of dissolved gases in natural waters. An application to thermal waters from Vulcano Island. *Applied Geochemistry*, 13(5), 631–642. [https://doi.org/10.1016/S0883-2927\(97\)00109-1](https://doi.org/10.1016/S0883-2927(97)00109-1)
- Cherniak, D. J., Watson, E. B., & Thomas, J. B. (2009). Diffusion of helium in zircon and apatite. *Chemical Geology*, 268(1–2), 155–166. <https://doi.org/10.1016/J.CHEMGEO.2009.08.011>
- Clarke, W. B., Jenkins, W. J., & Top, Z. (1976). Determination of tritium by mass spectrometric measurement of ^3He . *The International Journal of Applied Radiation and Isotopes*, 27(9), 515–522. [https://doi.org/10.1016/0020-708X\(76\)90082-X](https://doi.org/10.1016/0020-708X(76)90082-X)
- Crespo-Blanc, A., & Frizon de Lamotte, D. (2006). Structural evolution of the external zones derived from the Flysch trough and the South Iberian and Maghrebian paleomargins around the Gibraltar arc: A comparative study. *Bulletin de La Societe Geologique de France*, 177(5), 267–282.

<https://doi.org/10.2113/gssgfbull.177.5.267>

- Díaz, J., Gallart, J., & Carbonell, R. (2016). Moho topography beneath the Iberian-Western Mediterranean region mapped from controlled-source and natural seismicity surveys. *Tectonophysics*, 692, 74–85. <https://doi.org/10.1016/j.tecto.2016.08.023>
- Dyja-Person, V., Tarantola, A., Richard, A., Hibsich, C., Siebenaller, L., Boiron, M., et al. (2018). Metamorphic brines and no surficial fluids trapped in the detachment footwall of a Metamorphic Core Complex (Nevado-Filábride units, Betics, Spain). *Tectonophysics*, 727(January), 56–72. <https://doi.org/10.1016/j.tecto.2018.02.001>
- Faccenna, C., Piromallo, C., Crespo-Blanc, A., Jolivet, L., & Rossetti, F. (2004). Lateral slab deformation and the origin of the western Mediterranean arcs. *Tectonics*, 23(1). <https://doi.org/10.1029/2002TC001488>
- Fernández-Ibáñez, F., Soto, J. I., & Morales, J. (2005). Profundidad de la transición dúctil-frágil en la corteza de Béticas-Rif y Mar de Alborán. *Geogaceta*, 37, 155–158.
- Galindo-Zaldívar, J., Gil, A. J., Sanz de Galdeano, C., Lacy, M. C., García-Armenteros, J. A., Ruano, P., et al. (2015). Active shallow extension in central and eastern Betic Cordillera from CGPS data. *Tectonophysics*, 663, 290–301. <https://doi.org/10.1016/j.tecto.2015.08.035>
- García-Tortosa, F. J., López-Garrido, A. C., & Sanz de Galdeano, C. (2000). Présence du complexe tectonique Malaguide à l'est de Carthagène (zone interne Bétique, Espagne). *Comptes Rendus de l'Académie Des Sciences-Series IIA-Earth and Planetary Science*, 330(2), 139–146. [https://doi.org/10.1016/S1251-8050\(00\)00124-5](https://doi.org/10.1016/S1251-8050(00)00124-5)
- Gautheron, C., & Moreira, M. (2002). Helium signature of the subcontinental lithospheric mantle. *Earth and Planetary Science Letters*, 199(1–2), 39–47. [https://doi.org/10.1016/S0012-821X\(02\)00563-0](https://doi.org/10.1016/S0012-821X(02)00563-0)
- Gilfillan, S. M. V., Wilkinson, M., Haszeldine, R. S., Shipton, Z. K., Nelson, S. T., & Poreda, R. J. (2011). He and Ne as tracers of natural CO₂ migration up a fault from a deep reservoir. *International Journal of Greenhouse Gas Control*, 5(6), 1507–1516. <https://doi.org/10.1016/j.ijggc.2011.08.008>
- Gómez-Pugnaire, M. T., & Fernández-Soler, J. M. (1987). High-pressure metamorphism in metabasites from the Betic Cordilleras (S.E. Spain) and its evolution during the Alpine orogeny. *Contributions to Mineralogy and Petrology*, 95(2), 231–244. <https://doi.org/10.1007/BF00381273>
- Heit, B., Mancilla, F. de L., Yuan, X., Morales, J., Stich, D., Martín, R., & Molina-Aguilera, A. (2017). Tearing of the mantle lithosphere along the intermediate-depth seismicity zone beneath

- the Gibraltar Arc: The onset of lithospheric delamination. *Geophysical Research Letters*, 44(9), 4027–4035. <https://doi.org/10.1002/2017GL073358>
- Hyndman, R. D., & Klemperer, S. L. (1989). Lower-crustal porosity from electrical measurements and inferences about composition from seismic velocities. *Geophysical Research Letters*, 16(3), 255–258.
- Hyndman, R. D., & Shearer, P. M. (1989). Water in the lower continental crust: modelling magnetotelluric and seismic reflection results. *Geophysical Journal International*, 98(2), 343–365. <https://doi.org/10.1111/j.1365-246X.1989.tb03357.x>
- Inguaggiato, C., Censi, P., D'Alessandro, W., & Zuddas, P. (2016). Geochemical characterisation of gases along the dead sea rift: Evidences of mantle-CO₂ degassing. *Journal of Volcanology and Geothermal Research*, 320, 50–57. <https://doi.org/10.1016/j.jvolgeores.2016.04.008>
- Inguaggiato, S., & Rizzo, A. (2004). Dissolved helium isotope ratios in ground-waters: a new technique based on gas–water re-equilibration and its application to Stromboli volcanic system. *Applied Geochemistry*, 19(5), 665–673. <https://doi.org/10.1016/j.apgeochem.2003.10.009>
- Jähne, B., Heinz, G., & Dietrich, W. (1987). Measurement of the diffusion coefficients of sparingly soluble gases in water. *Journal of Geophysical Research: Oceans*, 92(C10), 10767–10776. <https://doi.org/10.1029/JC092iC10p10767>
- Janowski, M., Loget, N., Gautheron, C., Barbarand, J., Bellahsen, N., Van Den Driessche, J., et al. (2016). Neogene exhumation and relief evolution in the eastern Betics (SE Spain): Insights from the Sierra de Gador. *Terra Nova*, 29(2), 91–97. <https://doi.org/10.1111/ter.12252>
- Jolivet, L., Faccenna, C., Goffé, B., Burov, E., & Agard, P. (2003). Subduction tectonics and exhumation of High-pressure metamorphic rocks in the Mediterranean orogens. *American Journal of Science*, 303, 353–409. <https://doi.org/10.2475/ajs.303.5.353>
- Kipfer, R., Aeschbach-Hertig, W., Peeters, F., & Stute, M. (2002). Noble gases in lakes and ground waters. *Reviews in Mineralogy and Geochemistry*, 47(1), 615–700.
- Lehmann, B. E., Love, A., Purtschert, R., Collon, P., Loosli, H. H., Kutschera, W., et al. (2003). A comparison of groundwater dating with ⁸¹Kr, ³⁶Cl and ⁴He in four wells of the Great Artesian Basin, Australia. *Earth and Planetary Science Letters*, 211(3–4), 237–250. [https://doi.org/10.1016/S0012-821X\(03\)00206-1](https://doi.org/10.1016/S0012-821X(03)00206-1)
- Lippolt, H. J., & Weigel, E. (1988). ⁴He diffusion in ⁴⁰Ar-retentive minerals. *Geochimica et Cosmochimica Acta*, 52(6), 1449–1458. [https://doi.org/10.1016/0016-7037\(88\)90215-3](https://doi.org/10.1016/0016-7037(88)90215-3)
- López-Chicano, M., Cerón, J. C., Vallejos, A., & Pulido-Bosch, A. (2001). Geochemistry of thermal springs, Alhama de Granada (southern Spain). *Applied Geochemistry*, 16(9–10), 1153–1163.

[https://doi.org/10.1016/S0883-2927\(01\)00020-8](https://doi.org/10.1016/S0883-2927(01)00020-8)

- Mancilla, F. de L., Booth-Rea, G., Stich, D., Pérez-Peña, J. V., Morales, J., Azañón, J. M., et al. (2015). Slab rupture and delamination under the Betics and Rif constrained from receiver functions. *Tectonophysics*, 663, 225–237. <https://doi.org/10.1016/j.tecto.2015.06.028>
- Mancilla, F. de L., Heit, B., Morales, J., Yuan, X., Stich, D., Molina-Aguilera, A., et al. (2018). A STEP fault in Central Betics, associated with lateral lithospheric tearing at the northern edge of the Gibraltar arc subduction system. *Earth and Planetary Science Letters*, 486, 32–40. <https://doi.org/10.1016/j.epsl.2018.01.008>
- Martelli, M., Bianchini, G., Beccaluva, L., & Rizzo, A. (2011). Helium and argon isotopic compositions of mantle xenoliths from Tallante and Calatrava, Spain. *Journal of Volcanology and Geothermal Research*, 200(1–2), 18–26. <https://doi.org/10.1016/j.jvolgeores.2010.11.015>
- Martínez-Martínez, J. M., & Azañón, J. M. (1997). Mode of extensional tectonics in the southeastern Betics SE Spain Implications for the tectonic evolution of the periAlborn orogenic system. *Tectonics*, 16(2), 205–225.
- Oelkers, E. H., & Helgeson, H. C. (1988). Calculation of the thermodynamic and transport properties of aqueous species at high pressures and temperatures: Aqueous tracer diffusion coefficients of ions to 1000°C and 5 kb. *Geochimica et Cosmochimica Acta*, 52(1), 63–85. [https://doi.org/10.1016/0016-7037\(88\)90057-9](https://doi.org/10.1016/0016-7037(88)90057-9)
- Ozima, M., & Podosek, F. A. (2002). *Noble gas geochemistry (2nd Edition)*. Cambridge University Press. <https://doi.org/10.1017/CBO9781107415324.004>
- Palomeras, I., Villaseñor, A., Thurner, S., Levander, A., Gallart, J., & Harnafi, M. (2017). Lithospheric structure of Iberia and Morocco using finite-frequency Rayleigh wave tomography from earthquakes and seismic ambient noise. *Geochemistry, Geophysics, Geosystems*, 18, 1824–1840. <https://doi.org/10.1002/2016GC006679>.Received
- Platt, J. P., & Vissers, R. L. M. (1989). Extensional collapse of thickened continental lithosphere: a working hypothesis for the Alboran Sea and Gibraltar Arc. *Geology*, 17(6), 540–543. [https://doi.org/10.1130/0091-7613\(1989\)017<0540:ECOTCL>2.3.CO;2](https://doi.org/10.1130/0091-7613(1989)017<0540:ECOTCL>2.3.CO;2)
- Rizzo, A. L., Caracausi, A., Chavagnac, V., Nomikou, P., Polymenakou, P. N., Mandalakis, M., et al. (2016). Kolumbo submarine volcano (Greece): An active window into the Aegean subduction system. *Scientific Reports*, 6(February), 1–9. <https://doi.org/10.1038/srep28013>
- Rosell, O., Martí, A., Marcuello, À., Ledo, J., Queralt, P., Roca, E., & Campanyà, J. (2011). Deep electrical resistivity structure of the northern Gibraltar Arc (western Mediterranean): evidence of lithospheric slab break-off. *Terra Nova*, 23(3), 179–186. <https://doi.org/10.1111/j.1365->

- Rudnick, R. L., & Fountain, D. M. (1995). Nature and composition of the continental crust: a lower crustal perspective. *Reviews of Geophysics*, 33(3), 267–309. <https://doi.org/10.1029/95rg01302>
- Sano, Y., & Marty, B. (1995). Origin of carbon in fumarolic gas from island arcs. *Chemical Geology (Isotope Geoscience Section)*, 119, 265–274. [https://doi.org/10.1016/0009-2541\(94\)00097-R](https://doi.org/10.1016/0009-2541(94)00097-R)
- Sano, Y., & Wakita, H. (1985). Geographical distribution of $^3\text{He}/^4\text{He}$ ratios in Japan: Implications for arc tectonics and incipient magmatism. *Journal of Geophysical Research*, 90(10), 8729–8741. <https://doi.org/10.1029/JB090iB10p08729>
- Sanz de Galdeano, C. (1990). Geologic evolution of the Betic Cordilleras in the Western Mediterranean, Miocene to the present. *Tectonophysics*, 172, 107–119. [https://doi.org/10.1016/0040-1951\(90\)90062-D](https://doi.org/10.1016/0040-1951(90)90062-D)
- Sanz de Galdeano, C. (2008). The Cadiz-Alicante fault: an important discontinuity in the Betic Cordillera. *Revista de La Sociedad Geológica de España*, 21((1-2)).
- Spakman, W., & Wortel, R. (2004). A tomographic view on western Mediterranean geodynamics. *The TRANSMED Atlas-The Mediterranean Region from Crust to Mantle*, 31–52. https://doi.org/10.1007/978-3-642-18919-7_2
- Steiger, R. H., & Jäger, E. (1977). Subcommission on geochronology: Convention on the use of decay constants in geo- and cosmochemistry. *Earth and Planetary Science Letters*, 36, 359–362. [https://doi.org/10.1016/0012-821x\(77\)90060-7](https://doi.org/10.1016/0012-821x(77)90060-7)
- Thurner, S., Palomeras, I., Levander, A., Carbonell, R., & Lee, C. T. (2014). Ongoing lithospheric removal in the western Mediterranean: Evidence from Ps receiver functions and thermobarometry of Neogene basalts (PICASSO project). *Geochemistry, Geophysics, Geosystems*, 15(4), 1113–1127. <https://doi.org/10.1002/2013GC005124>
- Tolstikhin, I., Lehmann, B. E., Loosli, H. H., & Gautschi, A. (1996). Helium and argon isotopes in rocks, minerals, and related ground waters: A case study in northern Switzerland. *Geochimica et Cosmochimica Acta*, 60(9), 1497–1514. [https://doi.org/10.1016/0016-7037\(96\)00036-1](https://doi.org/10.1016/0016-7037(96)00036-1)
- Tolstikhin, I. N., Lehmann, B. E., Loosli, H. H., Kamensky, I. L., Nivin, V. A., Orlov, S. P., et al. (1999). Radiogenic helium isotope fractionation: the role of tritium as ^3He precursor in geochemical applications. *Geochimica et Cosmochimica Acta*, 63(10), 1605–1611. [https://doi.org/10.1016/S0016-7037\(99\)00105-2](https://doi.org/10.1016/S0016-7037(99)00105-2)
- Tolstikhin, I., Waber, H. N., Kamensky, I., Loosli, H. H., Skiba, V., & Gannibal, M. (2011). Production, redistribution and loss of helium and argon isotopes in a thick sedimentary aquitard-aquifer system (Molasse Basin, Switzerland). *Chemical Geology*, 286(1–2), 48–58.

<https://doi.org/10.1016/j.chemgeo.2011.04.017>

Tubía, J. M., Cuevas, J., Navarro-Vilá, F., Alvarez, F., & Aldaya, F. (1992). Tectonic evolution of the Alpujarride Complex (Betic Cordillera, southern Spain). *Journal of Structural Geology*, 14(2), 193–203. [https://doi.org/10.1016/0191-8141\(92\)90056-3](https://doi.org/10.1016/0191-8141(92)90056-3)

Vergés, J., & Fernández, M. (2012). Tethys – Atlantic interaction along the Iberia – Africa plate boundary: The Betic – Rif orogenic system. *Tectonophysics*, 579, 144–172. <https://doi.org/10.1016/j.tecto.2012.08.032>

Weiss, R. F. (1971). Solubility of helium and neon in water and seawater. *Journal of Chemical & Engineering Data*, 16(2), 235–241. <https://doi.org/10.1021/jc60049a019>

Table 1: Physical and Chemical Parameters of the Waters Sampling Sites and Helium Isotopic Composition of Dissolved and Bubbling Gases

| Sampling points ^a | Code | Ref. number | T (°C) | pH | EC ^b (mS/cm) | Alkalinity (x 10 ⁻³ mol/L) | Gas type ^c | He ^d | ³ He/ ⁴ He ^e | (³ He/ ⁴ He) _c ^f | ⁴ He/ ²⁰ Ne |
|--------------------------------|------|-------------|--------|-----|-------------------------|---------------------------------------|-----------------------|-----------------|---|---|-----------------------------------|
| Baños Santa Fe (W) | SF | 9 | 39 | 7.0 | 4.69 | 2.58 | D | 1.46E-3 (7) | 0.067 (2) | 0.024 (4) | 5.9 (3) |
| Sierra Elvira (S) | SE | 7 | 30 | 6.9 | 3.82 | 3.77 | D | 1.74E-3 (9) | 0.083 (2) | 0.057 (3) | 9.2 (5) |
| Vivero Arco (W) | VA | 8 | 17 | 7.1 | 2.01 | 7.44 | D | 9.1E-5 (5) | 0.44 (2) | na | 0.40 (2) |
| Baños Alicun de las Torres (S) | AT | 5 | 34 | 6.7 | 2.24 | 7.94 | D | 3.3E-3 (2) | 0.119 (4) | 0.106 (4) | 18.1 (9) |
| Baños Alhama de Granada (S) | BAG | 12 | 40 | 7.4 | 1.13 | 3.05 | D | 2.0E-3 (1) | 0.135 (4) | 0.105 (5) | 7.8 (4) |
| Baños Salado de Lanjaron (S) | BSL | 1 | 26 | 5.8 | 8.18 | 4.72 | D | 1.66E-4 (8) | 0.158 (5) | na | 1.04 (5) |
| Baños de Zujar (W) | BZ | 4 | 35 | 6.8 | 12.82 | 2.06 | D | 5.3E-3 (3) | 0.057 (2) | 0.049 (2) | 33 (2) |
| Salinas Malaha (S) | SM | 10 | 20 | 6.8 | 187.10 | 3.81 | D | nm | nm | na | nm |
| Baños Alhamilla (S) | BAA | 3 | 51 | 7.1 | 1.92 | 4.32 | D | 1.54E-3 (8) | 0.124 (4) | 0.071 (5) | 4.9 (2) |
| | | | | | | | B | 121 (6) | 0.108 (3) | 0.083 (4) | 10.5 (5) |
| Baños Urquizar Grande (S) | BUG | 11 | 23 | 7.3 | 1.50 | 2.89 | D | 6.2E-4 (3) | 0.096 (3) | 0.017 (7) | 3.0 (2) |
| | | | | | | | B | 46 (2) | 0.165 (5) | 0.06 (1) | 2.6 (1) |
| Capuchina Lanjaron (S) | CL | 2 | 21 | 6.1 | 34.15 | 12.87 | D | nm | nm | na | nm |
| | | | | | | | B | 3.1 (0.2) | 1.03 (3) | 1.1 (5) | 0.46 (2) |
| Frontil (S) | FR | 6 | 17 | 7.5 | 0.67 | 6.15 | B | 14.3 (7) | 0.43 (1) | 0.06 (8) | 0.72 (4) |

Notes. nm = not measured. na = not applicable.

1σ uncertainties are displayed as last significant figures in parentheses.

^aSample collected in: Spring (S) and Well (W).

^bEC: electrical conductivity.

^cB: bubbling gas. D: dissolved gas.

^dHelium concentrations are expressed in cm³ (STP)/L_{water} for dissolved gases and in ppmv for bubbling gases.

Standard conditions are p = 101.325 kPa and T = 25°C.

^eHelium isotopic composition is expressed as R/R_A, where R is the ³He/⁴He ratio of the samples normalised to the atmospheric ratio (R_A = 1.39 × 10⁻⁶).

^fHelium isotopic composition, expressed as R/R_A, corrected for the atmospheric contamination.

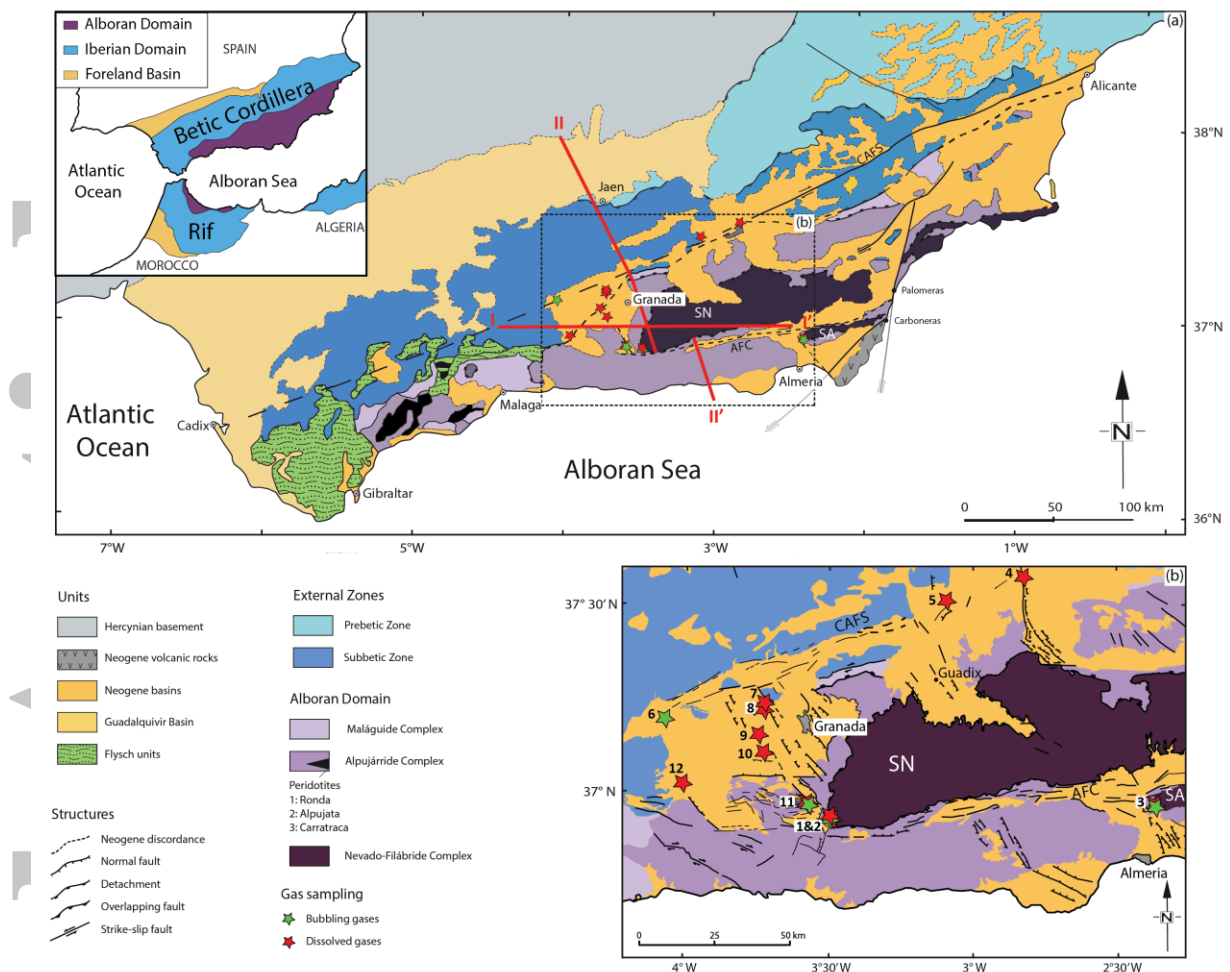


Figure 1: (a) Structural map of the Betic Cordillera (Spain) including the main lithological units and structures. Bold red lines shows the location of the cross-sections presented in Figure 2 and discussed in text. Structural map modified after Augier (2004). Inset indicates the main tectonic domains of the peri-Alboran orogenic system modified after Janowski et al. (2016). (b) Detailed structural map of the Central Betic Cordillera showing the main tectonic domains and faults. SN and SA are Sierra Nevada and Sierra Alhamilla massifs respectively. Sampling points are: (1) Baños Salado de Lanjaron, (2) Capuchina de Lanjaron, (3) Baños Alhamilla, (4) Baños Zujar, (5) Baños Alicun de las Torres, (6) Frontil, (7) Sierra Elvira, (8) Viviero Arco, (9) Baños Santa Fe, (10) Salinas la Malaha, (11) Baños Urquizar Grande and (12) Baños Alhama de Granada.

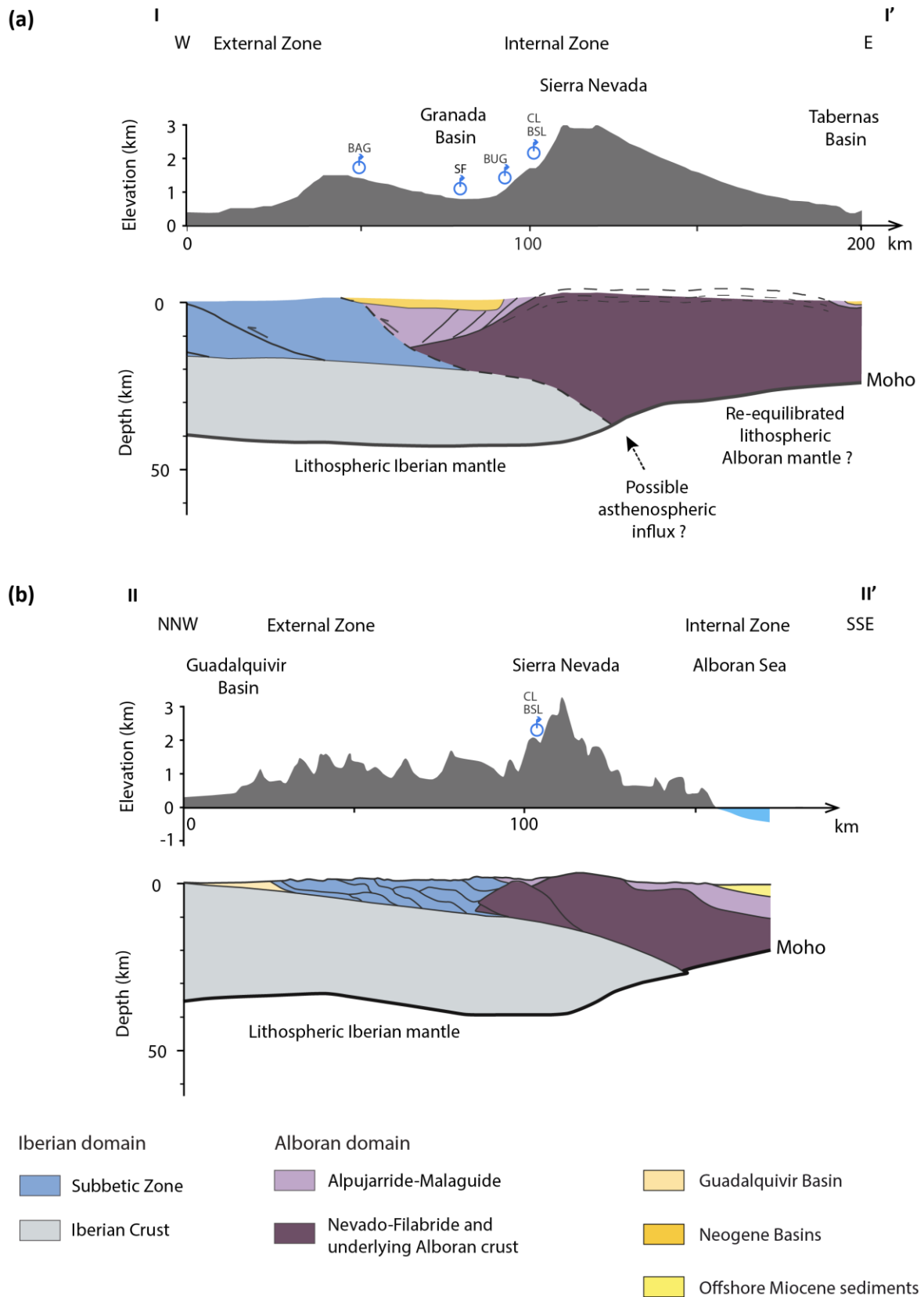


Figure 2: (a) Original W-E cross-section showing the lithospheric structure of the Betic Cordillera. Five sampling points have been projected on the topographic section. Moho

profile was constrained using Diaz et al. (2016)'s data from deep seismic sounding experiments and receiver functions studies. (b) NNW-SSE cross-section of the Betic Cordillera modified from Crespo-Blanc and Frizon de Lamotte (2006). Two sampling points have been projected on the topographic section.

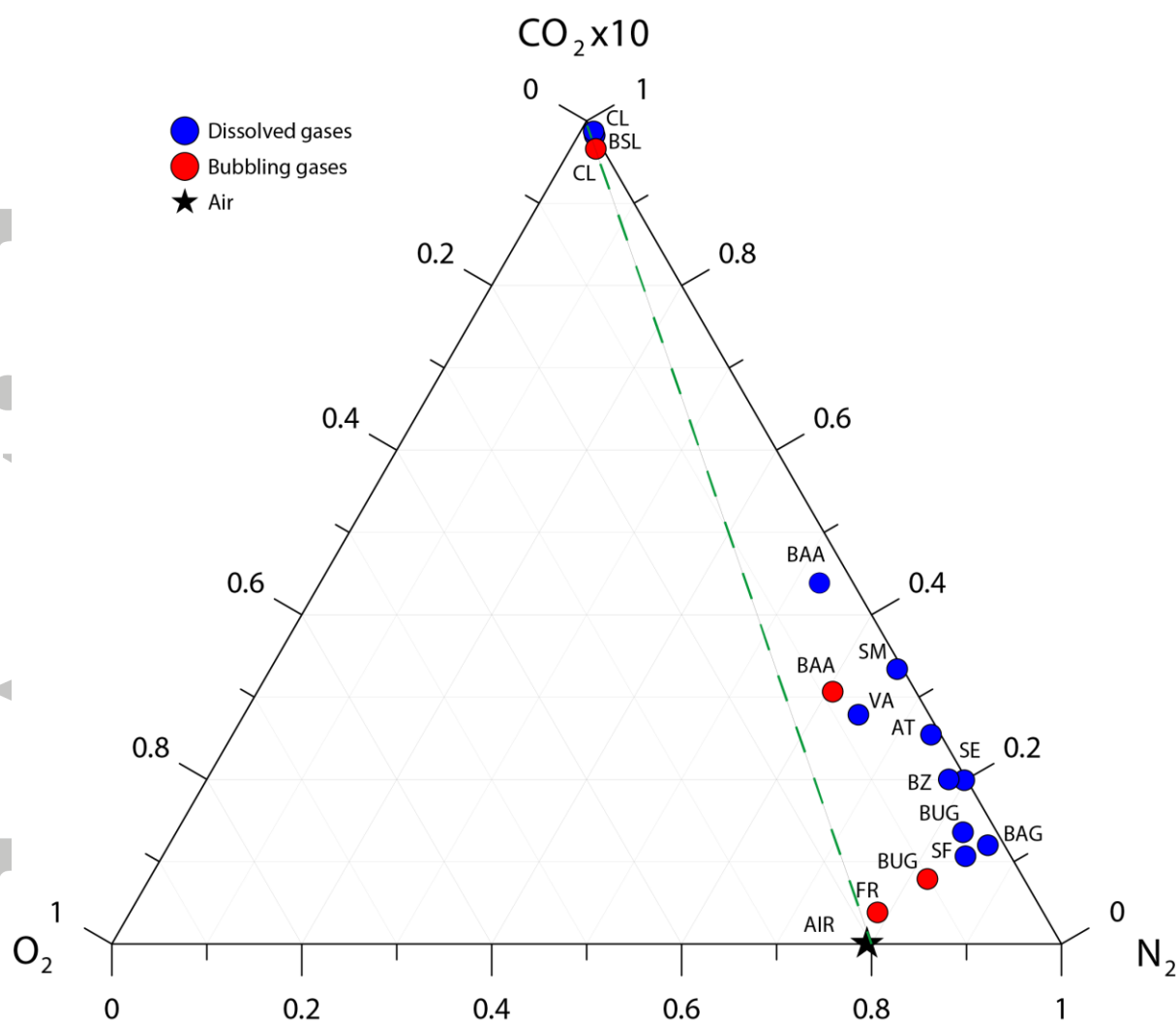


Figure 3: Triangular plot of the relative pressure of CO_2 , N_2 , and O_2 . The air value is also reported for comparison; the green dotted line represents the theoretical mixing between air dominated system and CO_2 -rich fluid.

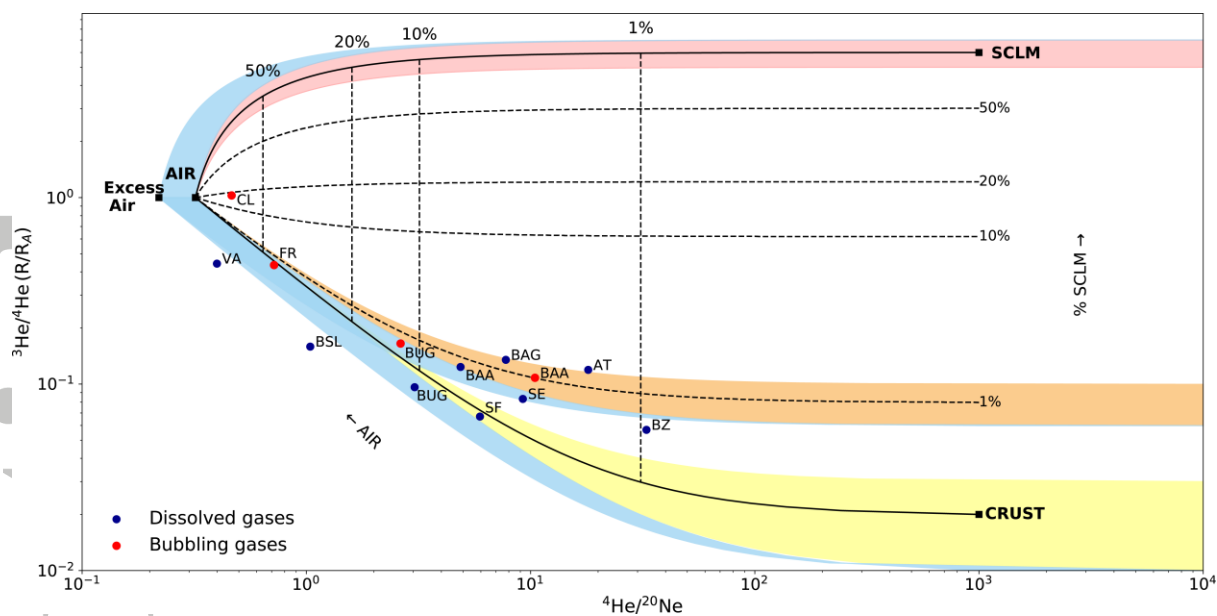


Figure 4: $^3\text{He}/^4\text{He}$ (R/R_A) values vs. $^4\text{He}/^{20}\text{Ne}$ ratios diagram. The uncertainties (1σ) are within the size of the symbols.

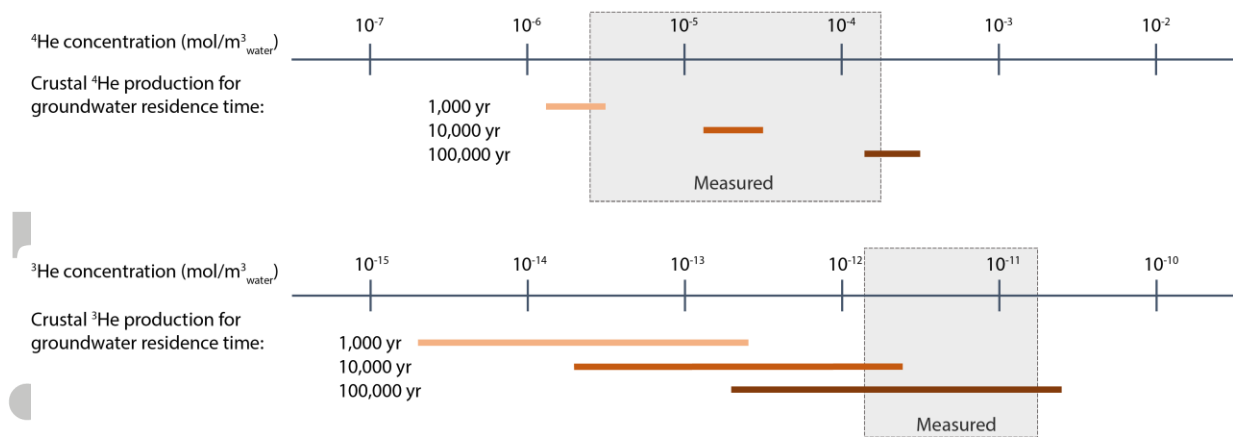


Figure 5: Comparison of ^4He and ^3He concentrations in water between measured and calculated values for groundwater residence time of 10^3 , 10^4 and 10^5 years. He concentrations in water from crustal production are calculated with the hypothesis of 3 % porosity.